JGR

RESEARCH ARTICLE

Key Points:
- Atmospheric lifetime of SF_6 reduced by nearly a factor of 3 based on measurements in the stratospheric polar vortex
- Consistency of SF_6 and HFC-227ea derived mean age of air gives independent confirmation of SF_6 lifetime reduction
- The signal of mesospheric loss or production of a trace gas is highly concentrated in the stratospheric polar vortices each winter

Quantification of the SF_6 lifetime based on mesospheric loss measured in the stratospheric polar vortex

Eric A. Ray[1,2] (iD), Fred L. Moore[2,3], James W. Elkins[3], Karen H. Rosenlof[1] (iD), Johannes C. Laube[4], Thomas Röckmann[5], Daniel R. Marsh[6] (iD), and Arlyn E. Andrews[3] (iD)

[1]Chemical Sciences Division, Earth Systems Research Laboratory, NOAA, Boulder, Colorado, USA, [2]Cooperative Institute for Research in Environmental Sciences, University of Colorado Boulder, Boulder, Colorado, USA, [3]Global Monitoring Division, Earth Systems Research Laboratory, NOAA, Boulder, Colorado, USA, [4]Centre for Ocean and Atmospheric Sciences, School of Environmental Sciences, University of East Anglia, Norwich, UK, [5]Institute for Marine and Atmospheric Research, Utrecht University, Utrecht, Netherlands, [6]Atmospheric Chemistry Observations and Modeling Laboratory, National Center for Atmospheric Research, Boulder, Colorado, USA

Abstract Sulfur hexafluoride (SF_6) is a greenhouse gas with one of the highest radiative efficiencies in the atmosphere as well as an important indicator of transport time scales in the stratosphere. The current widely used estimate of the atmospheric lifetime of SF_6 is 3200 years. In this study we use in situ measurements in the 2000 Arctic polar vortex that sampled air with up to 50% SF_6 loss to calculate an SF_6 lifetime. Comparison of these measurements with output from the Whole Atmosphere Community Climate Model (WACCM) shows that WACCM transport into the vortex is accurate and that an important SF_6 loss mechanism, believed to be electron attachment, is missing in the model. Based on the measurements and estimates of the size of the vortex, we calculate an SF_6 lifetime of 850 years with an uncertainty range of 580–1400 years. The amount of SF_6 loss is shown to be consistent with that of HFC-227ea, which has a lifetime of 670–780 years, adding independent support to our new SF_6 lifetime estimate. Based on the revised lifetime the global warming potential of SF_6 will decrease only slightly for short time horizons (<100 years) but will decrease substantially for time horizons longer than 2000 years. Also, the use of SF_6 measurements as an indicator of transport time scales in the stratosphere clearly must account for potential influence from polar vortex air.

Plain Language Summary We have calculated an atmospheric lifetime of the molecule SF_6 based on trace gas measurements in the stratospheric polar vortex. This lifetime is 3 times shorter than the commonly used lifetime over the past 20 years. Since SF_6 is a greenhouse gas this adjustment has implications for long-term climate effects.

1. Introduction

The trace gas sulfur hexafluoride (SF_6) is an anthropogenic, very long lived species in steady growth [*Carpenter et al.*, 2014; *Dlugokencky et al.*, 2016; *Hall et al.*, 2016] and has one of the highest radiative efficiencies of any molecule [e.g., *Ravishankara et al.*, 1993; *Hodnebrog et al.*, 2013]. As with many long-lived trace gases, SF_6 is destroyed at altitudes above 45 km in the middle atmosphere where a relatively small amount of mass is transported through the region of rapid chemical destruction. Measurements of trace gases in the mesosphere and above are rare and difficult to obtain, so direct confirmation of where and how SF_6 loss occurs is lacking.

The current widely used estimate of the atmospheric lifetime of SF_6 is 3200 years based primarily on loss due to Lyman-α photolysis [e.g., *Ravishankara et al.*, 1993]. This value has been used in all of the climate and stratospheric ozone assessments and State of the Climate report, even though *Ravishankara et al.* [1993] gave a large range of uncertainty from $580 <$ lifetime $< 10,000$ years. A number of studies have suggested that SF_6 destruction by free electron association is actually the dominant loss mechanism in the mesosphere [*Morris et al.*, 1995; *Reddmann et al.*, 2001; *Totterdill et al.*, 2015; *Kovács et al.*, 2017]. With the inclusion of destruction by electron association the SF_6 lifetime estimate can decrease to 600–800 years [*Ravishankara et al.*, 1993; *Morris et al.*, 1995], but a quantitative confirmation from observations has been missing so far.

Evidence of SF_6 loss has been seen in in situ balloon and aircraft observations [*Strunk et al.*, 2000; *Andrews et al.*, 2001; *Engel et al.*, 2002, 2006] as well as satellite measurements [*Haenel et al.*, 2015]. This loss is evident when SF_6 is used to calculate the stratospheric mean age of air, which is the time an air parcel has resided in

the stratosphere [e.g., *Waugh and Hall*, 2002]. When SF_6 based mean age is compared to mean age calculated from a trace gas with a longer atmospheric lifetime, such as CO_2, an older mean age derived for SF_6 is an indication of chemical loss of SF_6. The in situ measurements indicating SF_6 loss have primarily been from the high latitudes, either in the stratospheric polar vortex or in regions where there was outflow or remnants of the polar vortex. The stratospheric polar vortex is characterized by rapid descent, and the entire mass of the mesosphere descends into each polar vortex 2 or 3 times over each fall and winter [e.g., *Fisher et al.*, 1993; *Ray et al.*, 2002; *Plumb et al.*, 2003]. Thus, the stratospheric polar vortex contains a concentrated amount of air with mesospheric character and is a useful place to measure the effects of mesospheric chemistry without having to launch instruments into the mesosphere. Any trace gas with mesospheric loss will be depleted in air that is transported into and through the polar vortex and subsequently into the midlatitude and high-latitude lower stratosphere when the vortex breaks down each spring.

In this study we use in situ measurements from balloon flights during the 1999–2000 northern winter [*Ray et al.*, 2002] to derive SF_6 loss that occurred in the mesosphere. The northern polar vortex was relatively undisturbed that winter, with no sudden stratospheric warming and a vortex breakdown in late March. The balloon flight on 5 March 2000 therefore was unique in that it sampled isolated air within the vortex that had descended from the mesosphere throughout the depth of the profile.

2. Measurements and Model Output

The measurements used in this study are primarily from the Lightweight Airborne Chromatograph Experiment (LACE) instrument. LACE is a three-channel electron capture detector-gas chromatograph (ECD-GC) designed to operate at ambient pressure on a balloon gondola [*Moore et al.*, 2003]. LACE was flown on the Observations of the Middle Atmosphere (OMS) balloon gondola from Kiruna, Sweden (68°N) on 5 March 2000 as part of the SAGE III Ozone Loss and Validation Experiment (SOLVE). Profiles of SF_6, CO, H_2, and several other long-lived trace gases were measured by LACE with a vertical resolution of 300–600 m and precisions of 1–2% [*Ray et al.*, 2002]. We also used measurements of CO_2 from the Harvard instrument on the same OMS balloon flight [*Daube et al.*, 2002]. In situ temperature and pressure measurements used to calculate a density profile were taken by a Vaisala radiosonde on a separate balloon platform flown from Kiruna on the same day as the OMS flight.

Additional measurements in the polar vortex come from whole air samples taken from the Geophysica aircraft during the RECONCILE project in Kiruna, Sweden, in January–March 2010 [*von Hobe et al.*, 2013]. These samples were analyzed by a preconcentration system coupled to a Gas Chromatograph with Mass Spectrometric detection to obtain mixing ratios of a variety of long-lived trace gases, including SF_6, HFC-227ea [*Laube et al.*, 2010, 2013], and so far unpublished data for octafluoropropane (C_3F_8). The fully fluorinated compound C_3F_8 has a very long atmospheric lifetime of ~7000 years [*Carpenter et al.*, 2014]. HFC-227ea, or 1,1,1,2,3,3,3-heptafluoropropane, is a CFC replacement gas currently exhibiting strong growth and has a stratospheric lifetime of 670–780 years [*Laube et al.*, 2010; *Carpenter et al.*, 2014; *Stratospheric Processes and their Role in Climate* (*SPARC*), 2013]. For this 2010 data set the average measurement precision was 1.7% for HFC-227ea and C_3F_8 and 0.8% for SF_6.

Model output presented here is from an updated version of the Whole Atmosphere Community Climate Model (WACCM) [*Marsh et al.*, 2013], the atmospheric component of National Center for Atmospheric Research's (NCAR) Community Earth System Model [*Hurrell et al.*, 2013]. The model's dynamical fields (temperature, zonal and meridional winds, and surface pressure) are specified in the troposphere and stratosphere from the Modern Era Retrospective Analysis for Research and Applications (MERRA) [*Rienecker et al.*, 2011]. This new version has an updated chemical scheme described in *Solomon et al.* [2015] and modification to parameterized gravity waves that improves circulation and temperature biases throughout the middle atmosphere [*Garcia et al.*, 2017]. WACCM has 88 vertical levels from the surface to 4.5×10^{-6} hPa (approximately 140 km) and has a horizontal resolution of 1.9° latitude by 2.5° longitude. This simulation followed the "REFC1D" protocol of the Chemistry Climate Model Initiative [*Eyring et al.*, 2013] for the specification of time-dependent greenhouse gases and ozone depleting substances. It should be noted that the only loss mechanism of SF_6 in the WACCM model is via photolysis in the spectral band 116 to 180 nm. Absorption cross sections used to calculate this loss are from *Pradayrol et al.* [1996], and the solar spectral irradiance varies as observed on a daily basis based on the empirical model of *Lean et al.* [2005]. This version of WACCM does not

include the removal of SF_6 by electron attachment, which is considered in the recent study by *Kovács et al.* [2017]; and therefore, the modeled lifetime of SF_6 in the upper atmosphere shown here should be longer than observed.

3. SF_6 Loss and Lifetime

In order to derive the atmospheric lifetime of any trace gas, the annual loss of the gas must be either inferred through measurements [e.g., *Volk et al.*, 1997] or modeled [*SPARC*, 2013]. In the case of measurement-derived loss, multiple trace gases must be used in order to reference the loss of one trace gas to that of another trace gas with a known lifetime [*Volk et al.*, 1997]. In the case of model estimates of trace gas lifetimes, the instantaneous loss can be calculated at each model time step and the lifetime calculated precisely. However, potential biases in the modeled transport of air through the loss region compared to the real atmosphere are an important source of uncertainty in such estimates of trace gas lifetimes. In this study we calculate the lifetime of SF_6 based on measurements taken in the northern stratospheric polar vortex during winter, where air from the mesosphere is known to descend and accumulate in relative isolation [*Fisher et al.*, 1993]. The technique we use to calculate the SF_6 lifetime takes advantage of the transport of air from the loss region of SF_6 in the mesosphere and above into the stratospheric polar vortex.

An initial aspect of our SF_6 lifetime calculation is to assess whether our measurements sampled mesospheric air in the stratospheric Arctic vortex and how representative the measured profile was of average vortex conditions. One way to make this assessment is to compare our measurements with modeled CO and H_2 profiles in the vortex. Both CO and H_2 are photochemically produced in the mesosphere [*Minschwaner et al.*, 2010; *Harries et al.*, 1996] and thus any increase in the mixing ratio above the stratospheric values of these trace gases is a distinct signature of mesospheric air. Figure 1 shows the measured profiles from the 5 March 2000 flight and WACCM output averaged from 70 to 90°N for the months of January, February, and March 2000. The descent of relatively high mixing ratios of CO and H_2 over the winter is clear from the WACCM output, and the measured profiles generally fall between the February and March modeled profiles. In mid-March the upper levels of the vortex began to break up so midlatitude air mixed into the high latitudes and altered the shape of the modeled profiles above 28 km. Since the measurements took place in early March it is not expected that they should agree with the model averages at all levels over the whole month of March. However, the similar increase in the measured and modeled CO and H_2 indicates that the measured profile was generally representative of the vortex as a whole and that we sampled mesospheric air at altitudes above roughly 18–20 km. Profiles of SF_6 and CO_2 are also shown in Figure 1, and they both differ significantly from the WACCM profiles. The decrease in SF_6 as a function of height is the signal of mesospheric loss that we will discuss further below. The difference between the measured and modeled CO_2 is primarily due to the too young age of air in the model vortex by ~1.5 years (not shown). This mean age difference based on the growth rate of CO_2 accounts for the ~3 ppm difference above 20 km. This model mean age bias in the polar vortex does not affect our calculation of the SF_6 lifetime.

Further evidence for the representativeness of our measured profile can be estimated by the position of the balloon flight within the vortex and the horizontally well mixed nature of the stratospheric polar vortex, especially during the winter of 1999–2000 [*Gao et al.*, 2002; *Ray et al.*, 2002]. The equivalent latitude profile of the vortex edge was estimated from the maximum horizontal potential vorticity gradients [e.g., *Dunkerton et al.*, 1981] based on MERRA reanalysis output (Figure 2). This equivalent latitude profile is representative of the average vortex edge position over the 2 to 3 weeks prior to the 5 March flight. We also used the vortex size estimates for the 1999–2000 northern winter from *Manney and Sabutis* [2000] and *Harvey et al.* [2002] as consistency checks and to help estimate the uncertainties. The equivalent latitude profile of the balloon flight, calculated from MERRA, is also included in Figure 2. The balloon equivalent latitudes are higher than the vortex edge values at all altitudes above ~16 km, and thus, the profile above that level was within the polar vortex. Below ~18 km on 5 March 2000 the polar vortex was longitudinally distorted and the balloon at these lower altitudes was positioned within the vortex edge region or between the main body of the vortex and a large piece of the vortex that was shed off. Thus, the balloon equivalent latitudes below 16 km in Figure 2 are lower than the vortex edge values but likely still in an air mass that was recently influenced by the vortex.
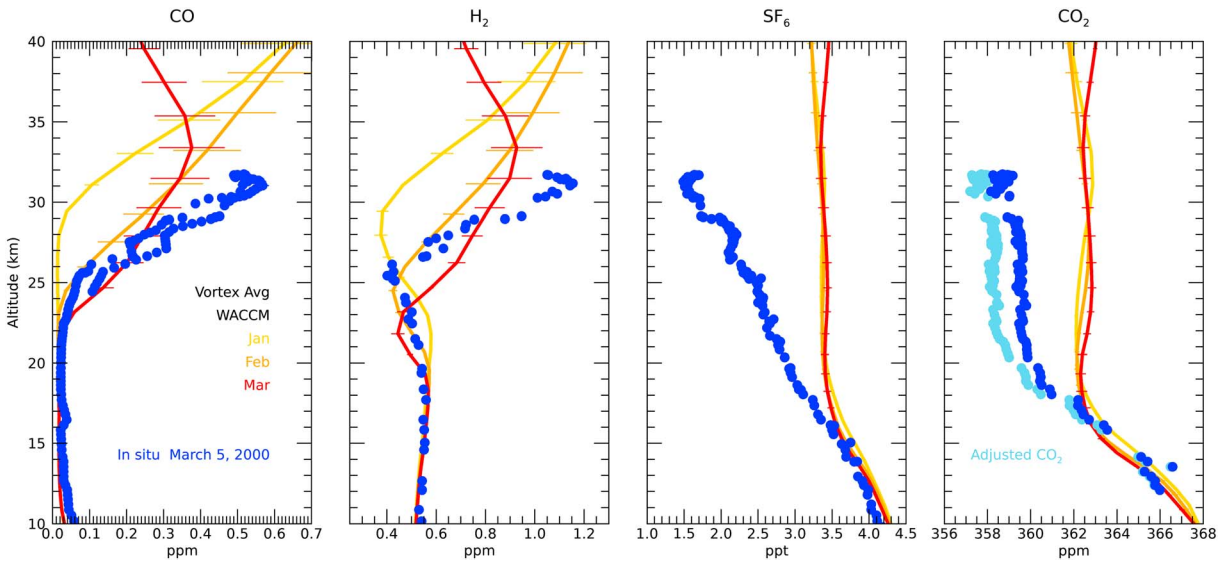
Figure 1. Profiles of CO, H_2, SF_6, and CO_2 in the northern stratospheric polar vortex measured by the LACE instrument (blue) during the SOLVE campaign on 5 March 2000 and from average WACCM output for January (yellow), February (orange), and March (red) 2000. The adjusted CO_2 profile is used in the calculation of mean age from CO_2 and takes into account production from CH_4 oxidation and loss from photolysis in the mesosphere. The WACCM profiles are made from averages over all latitudes and longitudes north of 70°N each month. Error bars on the WACCM profiles represent the standard deviation for each average. Error bars are also included on the measurements but are almost always smaller than the size of the symbol.

Horizontal mixing within the vortex can be inferred from the calculation of the equivalent length [e.g., *Haynes and Shuckburgh*, 2000]. Equivalent length is a dimensionless quantity calculated here from MERRA potential vorticity. Figure 3 shows distributions of equivalent length as a function of equivalent latitude averaged from 1 February to 5 March 2000 for three potential temperature levels, 500, 650, and 800 K, which correspond to 20, 24, and 28 km altitudes in the vortex. The notable features of these distributions are maxima in the midlatitudes and the polar vortex and a minimum in the vortex edge region. The midlatitude winter surf zone is a region of strong mixing, corresponding to the large values of equivalent length. The secondary maximum in equivalent length within the polar vortex suggests this
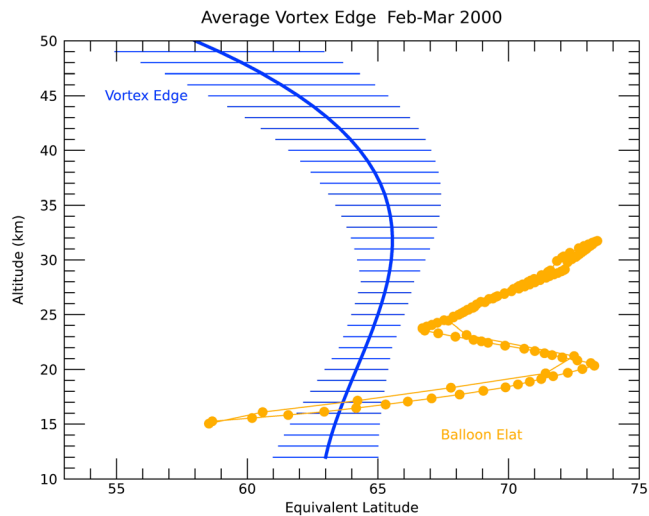
Figure 2. Equivalent latitude profile of the polar vortex edge for late February through early March 2000 used to calculate the area of the vortex. The equivalent latitude of the edge was determined from MERRA potential vorticity gradients as well as from previous studies of vortex size (see text). The error bars represent an uncertainty in the exact value of the potential vorticity gradient that best represents the vortex edge as well as the fact that the vortex edge is typically a region rather than a single location. The equivalent latitude of the 5 March 2000 balloon profile, also estimated from MERRA2, is shown in the orange symbols.
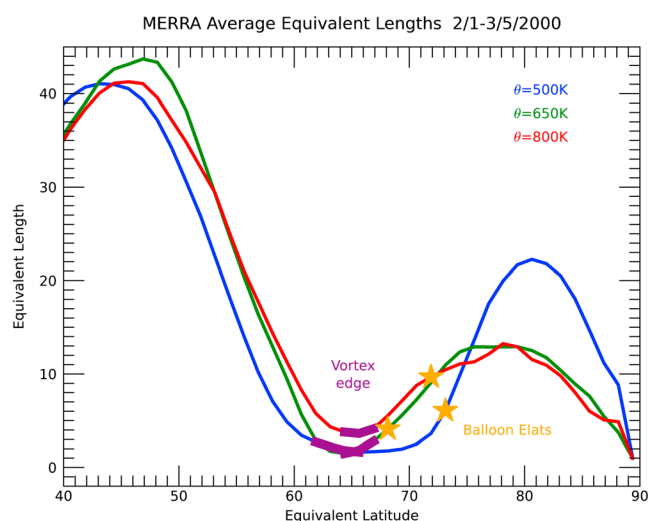
Figure 3. Average equivalent lengths as a function of equivalent latitude for the period 1 February to 5 March 2000 at three different potential temperature levels, 500 K in blue, 650 K in green, and 800 K in red. The equivalent length is an indicator of horizontal mixing. The vortex edge regions with uncertainties and the balloon position at each potential temperature level based on Figure 2 are shown in purple and orange, respectively.

is also a well-mixed environment. The polar vortex edge is an effective barrier to mixing and so corresponds with relatively low values of equivalent length. The vortex edge estimates in Figure 2 correspond well with the locations of the minimums in the equivalent length distributions.

As will be discussed below, of relevance to our calculation of SF_6 loss in the vortex is whether the vortex was well mixed all the way to the edge. This would imply that the SF_6 loss we measured was representative of the loss throughout the vortex area. We cannot prove conclusively that this was the case but there is evidence to suggest this is a reasonable assumption. Primarily, the fact that the position of the balloon profile within the vortex was always within 2–7° of the edge and not in the region of maximum mixing (Figure 5). Yet, long-lived tracer-tracer correlation curves based on in situ measurements from the same balloon flight are compact and distinct from midlatitude curves at all altitudes [*Ray et al.*, 2002], which can only occur in a horizontally well mixed vortex. Further evidence for a well-mixed polar vortex up to the edge is seen in satellite trace gas measurements from other northern winters, such as N_2O from the Microwave Limb Sounder (MLS) [*Manney and Lawrence*, 2016]. The MLS N_2O measurements have almost no gradient in equivalent latitude within the entire vortex. Thus, we assume the vortex is well mixed to the edge but includes an uncertainty in the vortex edge position to account for the uncertainty in the well-mixed area of the vortex.

To derive the measured loss of SF_6 in the vortex, it is necessary to first calculate the mean age of air from SF_6 and from another very long lived trace gas in growth, in this case we use CO_2 (Figure 1). A particular sample volume of stratospheric air can be described as a collection of infinitesimal particles, and the age of air refers to the time an individual particle has resided in the stratosphere. The distribution of particle ages is known as the age spectrum, with the average of the distribution referred to as the mean age of air [*Kida*, 1983; *Hall and Plumb*, 1994]. The shape of the age spectrum is determined by the zonal mean overturning, or Brewer-Dobson, circulation, which produces a young leading edge of the spectrum, and horizontal mixing of air between the polar latitudes, midlatitudes, and tropics, which produces an old age tail of the spectrum. The mean age of air can be calculated from trace gas measurements, typically by a time lag technique applied to roughly linearly growing trace gases that are nearly inert in the stratosphere [e.g., *Schmidt and Khedim*, 1991].

In this study we calculated mean ages from the SF_6 and CO_2 measurements based on the convolution of age spectra with the tropical tropopause time series of each trace gas, which accounts for nonlinear growth of the trace gas. Following *Hall and Plumb* [1994], the mixing ratio of a trace gas in the stratosphere in the absence of loss is defined as
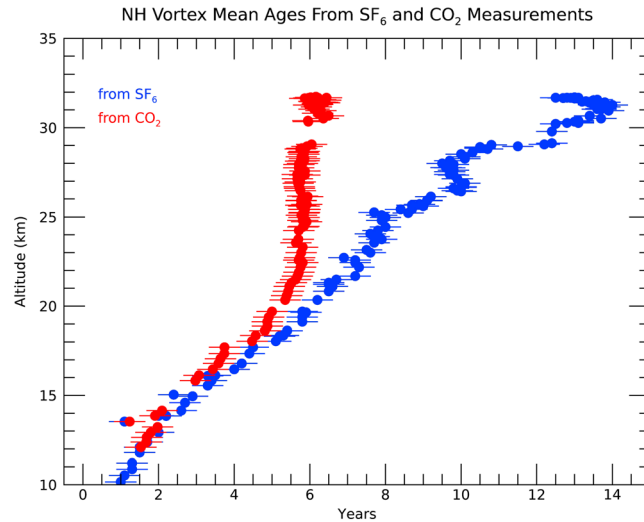
Figure 4. Profiles of the mean age of air derived from CO_2 (red) and SF_6 (blue) in situ measurements. The mean age differences are used to derive the SF_6 loss that accumulated in the vortex (see text). Error bars are based on uncertainties in the measurements of the trace gases, the reference tropical tropopause time series of each gas, and in the approximation of the age spectra in the calculation of mean age.

$$\chi_i(P,t) = \int_{t-\Delta t}^{t} \chi_i\left(P_o, t - t'\right) G_i\left(P, t - t'\right) dt' \tag{1}$$

where χ is the tracer mixing ratio, the i subscript refers to a particular trace gas, P is a location in the stratosphere, P_o is the tropical tropopause location, G is the age spectrum, t is time, t' is a time before t, and Δt is the total length of the age spectrum, which is 25 years in this case. We use an inverse Gaussian function for the shape of G where the mean age (Γ) scaled by a constant factor of 0.8 determined the width of the function [e.g., *Waugh and Hall*, 2002]. The tropical tropopause time series are based on the combined SF_6 data from the NOAA/ESRL Global Monitoring Division and Globalview tropical average marine boundary layer CO_2 [*Cooperative Global Atmospheric Data Integration Project*, 2013]. For each trace gas we calculated stratospheric mixing ratios χ based on equation (1) and a range of age spectra G with mean ages from 0 to 15 years. Based on the best matches between the measured and calculated stratospheric trace gas mixing ratios we separately find the best G_{SF6} and G_{CO2} and associated Γ_{SF6} and Γ_{CO2} as shown in Figure 4.

The profiles of Γ_{SF6} and Γ_{CO2} (Figure 2) show similar values in the lower stratosphere and relatively older SF_6 mean ages with increasing height. The nearly constant CO_2 mean ages of 5–6 years above 20 km are consistent with what we expect from many previous measurement-based estimates of mean age in the midlatitude and high latitude [*Engel et al.*, 2009; *Ray et al.*, 2014]. CO_2 is conserved in the stratosphere except for a small source from CH_4 oxidation; however, in the mesosphere ultraviolet photodissociation of CO_2 to CO represents a significant loss [*Minschwaner et al.*, 2010]. When computing mean age from CO_2 these processes are taken into account by making adjustments to the CO_2 mixing ratio before calculating the mean age using simultaneous measurements of CH_4 and CO. To adjust for the production of CO_2 from CH_4 oxidation we assume that the difference between the measured CH_4 mixing ratio in the stratosphere and the tropical tropopause CH_4 mixing ratio, from NOAA/ESRL surface measurements, was all converted into CO_2. To adjust for the photolysis of CO_2 into CO we assume that measured stratospheric CO above a background value of 50 ppb was produced from CO_2. The measured and adjusted CO_2 profiles are shown in Figure 1. Note that CO_2 photolysis in the mesosphere is not a permanent sink for CO_2 since the CO will eventually be oxidized by reaction with OH to reform CO_2 when the air descends to lower altitudes. The mean age calculated from CO_2 is assumed to represent the "true" mean age of air within the uncertainty of the calculation, which is approximately 3–6 months [e.g., *Engel et al.*, 2009; *Ray et al.*, 2014]. The mean age calculated from a long-lived trace gas with photochemical loss will have a bias toward an apparent older mean age due to the loss. The photochemical loss translates into an older mean age since the mean age is calculated based on the growth of the trace gas and so for a
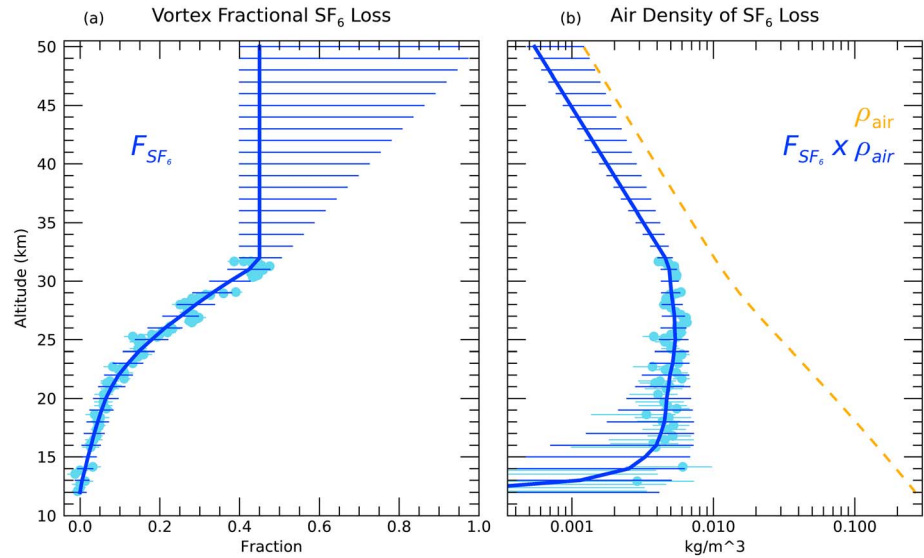
Figure 5. (a) Profile of the fractional loss of SF_6 accumulated in the vortex based on in situ measurements (light blue circles). The dark blue line represents a fit through the measured loss with a constant extrapolation through the upper stratosphere above where measurements could be taken. The error bars in the altitude range where measurements were taken represents the spread in the measured SF_6 loss. The loss extrapolation above the maximum observed altitude has error bars that remain constant at the observed uncertainty on the small end and increase with height on the larger end to a value of 100% SF_6 loss at the top of the vortex. (b) Profiles of the density of air in the vortex (orange line) and the fractional loss of SF_6 in the vortex multiplied by the density of air (blue line and light blue circles).

gas with linearly increasing concentration in the troposphere, a relatively low mixing ratio corresponds to a relatively longer time since that mixing ratio was present at the tropical tropopause, and thus an older mean age. The apparent SF_6 mean ages of up to 14 years near the top of the profile are a clear indication of loss of SF_6.

The difference between Γ_{SF6} and Γ_{CO2} can be translated into an amount of SF_6 loss by calculating an idealized "no loss" profile of SF_6 (χ_{SF6nl}). To calculate χ_{SF6nl}, we use equation (1) with the SF_6 tropical tropopause time series and the age spectra based on the CO_2 mean age for each measurement location:

$$\chi_{SF_6nl}(P, t) = \int_{t-\Delta t}^{t} \chi_{SF_6}\left(P_o, t - t'\right) G_{CO_2}\left(P, t - t'\right) dt' \tag{2}$$

From the χ_{SF6nl} profile the fractional loss profile of SF_6 (F_{SF6}) was calculated by

$$F_{SF_6} = \left(\chi_{SF_6nl} - \chi_{SF_6}\right) / \chi_{SF_6nl} \tag{3}$$

The values of F_{SF6} range from zero in the lower stratosphere up to nearly 0.5, or 50% loss of SF_6, in the middle stratosphere (Figure 5a). Without measurements in the upper half of the vortex we need to approximate the loss in that region. To estimate uncertainty, we investigate two extreme scenarios, one where the loss stays constant at the value found in the middle stratosphere, and a second one where the loss increases linearly to a value of one, which means all of the SF_6 would be lost at the top of the vortex. The constant loss scenario in the upper stratospheric vortex is thought to be most likely based on WACCM output that suggests roughly constant mesospheric influence in this region (not shown). The two upper stratospheric scenarios span a large range of loss fractions in the upper vortex, but given the relatively low density of air in that region compared to the lower stratosphere the difference between the two scenarios regarding the overall SF_6 loss is small (Figure 5b).

Based on the derived fractional SF_6 loss in the vortex we can now estimate the total atmospheric fractional SF_6 loss per year with the following equation:
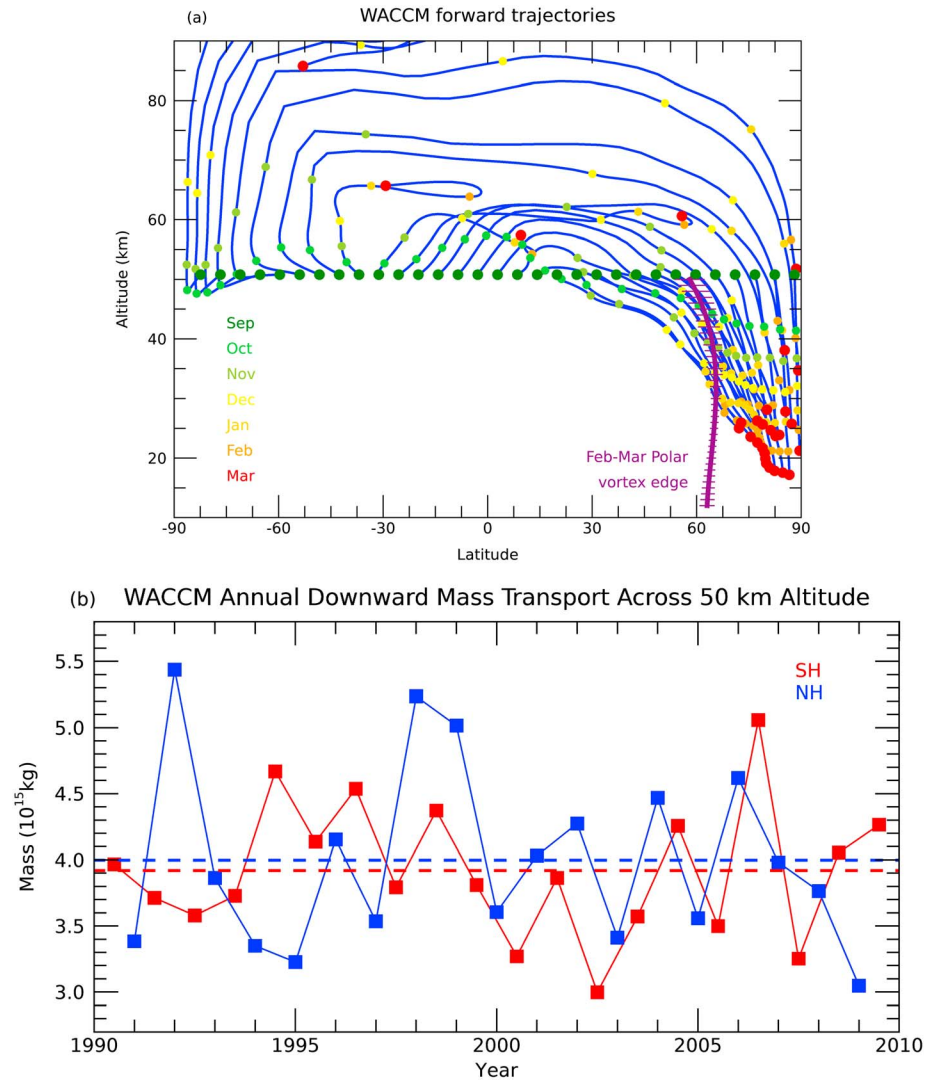
Figure 6. (a) Forward trajectories from September 1999 to March 2000 based on the WACCM residual circulation. The trajectories were initialized at an altitude of 50 km and all latitudes (green circles). Red circles indicate final trajectory positions in March 2000, and colored circles denote the individual months on each trajectory. The polar vortex edge in late February through early March is shown by the purple line and is equivalent to Figure 2. (b) Time series of the annual total downward mass transported across the 50 km altitude level poleward of 30° in each hemisphere. The NH annual totals are taken from July to June, and the SH totals are taken from January to December each year. So the NH value for 2000 is the total from July 1999 to June 2000. A dashed line indicates the 20 year average for each hemisphere. Note that the total mass of the atmosphere above 50 km (~1 hPa) is 1.3×10^{15} kg so that on average 3 times the mass of the entire mesosphere is transported into each polar vortex each year.

$$L_{SF6} = 2\int_{Z_b}^{Z_t} A_v(z)\rho(z)F_{SF6}(z)dz / M_A \qquad (4)$$

where z_b and z_t are the altitudes of the bottom and top of the vortex (values of 12 and 50 km were used here), A_v is the area of the vortex, ρ is the density of air, F_{SF6} is the fractional loss of SF_6 in the vortex, and M_A is the total mass of the atmosphere (5.148×10^{18} kg). The density profile is obtained from a combination of in situ measurements of temperature and pressure in the polar vortex up to 32 km from a Vaisala radiosonde flown nearly simultaneously to the OMS balloon, and WACCM average vortex temperatures and pressures above 32 km. The area of the vortex, A_v, is estimated based on the vortex edge profile shown in Figure 2.

To account for the descent of mesospheric air into both the northern and southern vortices every year, there is a factor of 2 in equation (4). This assumption of roughly equal descent into the southern and northern vortices is supported by trajectory and mass flux calculations from the WACCM residual circulation. Figure 6a

shows forward trajectories initialized at an altitude of 50 km and at all latitudes on September 1999 and run for 6 months to March 2000. The rapid pole-to-pole transport in the mesosphere is apparent as well as the accumulation of mesospheric air deep into the polar vortex. The forward trajectory calculation does not include mixing, so some of the mesospheric air that descended into the vortex may have been mixed out into the midlatitudes. In our calculation, mesospheric air that was mixed out of the vortex, or mesospheric air that descended outside the vortex, would be unaccounted for SF_6 loss and would bias our lifetime estimate too high. Forward trajectories initialized in March and run to September are reversed, so they descend into the southern vortex (not shown). To compare the descent of mesospheric air into each hemisphere, we calculated the total annual mass that crossed the 50 km altitude level south of 30°S and north of 30°N for each year from 1990 to 2010 (Figure 6b). There is variability from year to year, but on average over the 20 year period the downward mass transport across 50 km is essentially the same in each hemisphere (dashed lines in Figure 6b). Also, in the year 2000 the descent into each hemisphere is very similar. This supports our assumption of roughly equal descent in each hemisphere in equation (4). However, this does not imply that, in general, the northern and southern polar vortices will contain the same signal, or amount, of mesospheric air. The size and stability of the southern polar vortex are greater than for the northern polar vortex, so the mesospheric air that has descended into the southern vortex is both distributed over a larger volume and typically more confined over the fall and winter compared to the mesospheric air that has descended into the northern vortex. This can be seen in satellite measurements of long-lived tracers, such as those of SF_6 and inferred mean age from the MIPAS instrument [*Haenel et al.*, 2015] where the average SF_6 mixing ratios are significantly lower in the southern vortex compared to the northern vortex. The confinement of mesospheric air in the polar vortex is only important for obtaining a representative sample of the descended SF_6 loss with a single balloon profile. But the confinement of air in the polar vortex is not important to the lifetime of SF_6 since only the mass flux through the loss region in the mesosphere is relevant.

Our best estimate of the SF_6 lifetime based on equation (4) is 850 years. The two main sources of uncertainty that we can quantify are uncertainties in the SF_6 loss fraction in the vortex and in the size of the vortex. The SF_6 lifetime uncertainty due to loss uncertainty is −200 to +400 years and ±100 years due to the vortex size uncertainty. The asymmetric uncertainty in the lifetime due to loss is due to the asymmetric uncertainty in the upper stratospheric loss profile above the level of measurements (Figure 5). The full range of possible lifetimes due to the combination of these uncertainties is 580–1400 years. A limitation of our lifetime estimate that we cannot quantify is the amount of air with SF_6 loss that does not descend into the polar vortex. This is SF_6 loss that is missed in our calculation, so it would lead to a lower lifetime. Thus, our lifetime estimate range could be considered an upper limit.
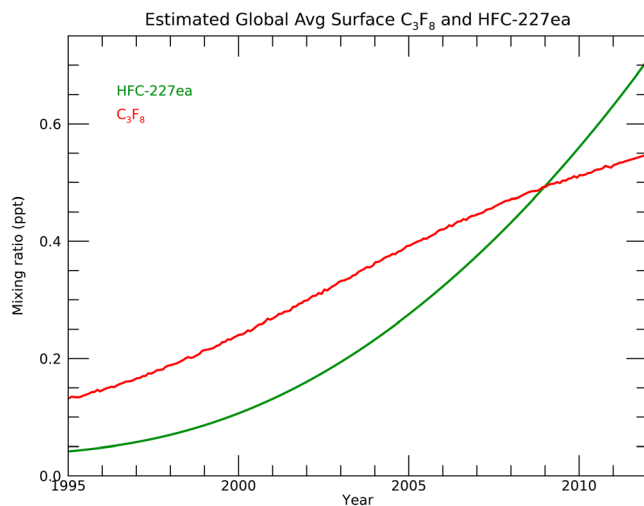
As mentioned in section 1, the currently accepted value of the SF_6 lifetime, since the *Ravishankara et al.* [1993] paper was published, is 3200 years. That paper and others since then [*Morris et al.*, 1995; *Reddmann et al.*, 2001; *Totterdill et al.*, 2015] have suggested that destruction of SF_6 by electron attachment is important and could result in a lifetime in the 550–800 year range. This lifetime range is consistent with the lower range of our estimate, which appears to validate the importance of electron attachment as the dominant SF_6 loss process. The only other known loss mechanism of significance for SF_6 is photolysis in the upper mesosphere. As an indication that photolysis cannot be the most important loss mechanism for SF_6 we compare the measurement-based SF_6 loss fraction in the polar vortex to the WACCM loss fraction averaged over latitudes poleward of 70°N (Figure 7). The WACCM SF_6 loss fraction was derived in a similar manner as was done for the measurements. First, "no loss" SF_6 mixing ratios were calculated based on the mean age from the WACCM idealized linear growth tracer. Then, the no loss SF_6 mixing ratios were subtracted from the model SF_6 mixing ratios and divided by the no loss SF_6 to get a loss fraction. Figure 7 clearly shows that the WACCM SF_6 loss in the polar vortex is much less than derived from measurements. WACCM vortex average SF_6 loss fractions are generally less than 0.1. Only above altitudes of 65 km are the WACCM SF_6 loss fractions greater than 0.4, while the measured loss fractions reach that value near 30 km altitude.

Independent measurement-based evidence for an SF_6 lifetime of less than 1000 years comes from in situ aircraft observations in the polar vortex of C_3F_8 and HFC-227ea. As for SF_6 and CO_2, C_3F_8 and HFC-227ea are trace gases that are in growth and long lived in the stratosphere so that mean age can be calculated from measured stratospheric mixing ratios compared to their time series of surface mixing ratios. We use the same technique to calculate the mean age from these species as was described earlier in the text for SF_6 and CO_2.
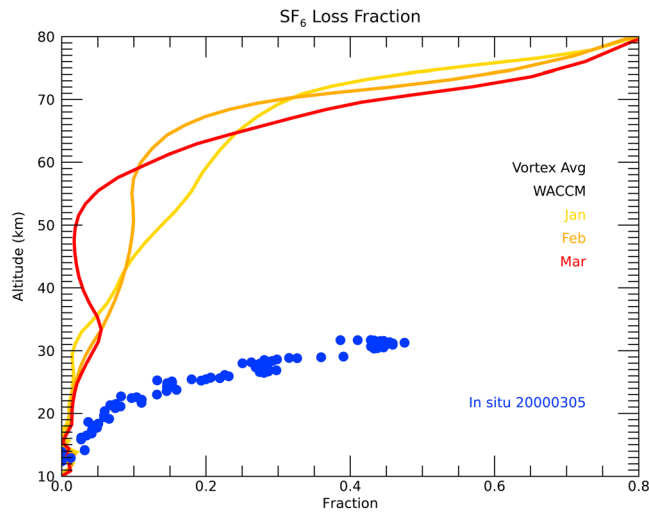
Figure 7. Profiles of SF_6 loss fraction from in situ measurements in the polar vortex (blue symbols, same as in Figure 5a) on 5 March 2000 and from WACCM averaged poleward of 70°N for the months of January (gold), February (orange), and March (red line) 2000.

These species have been measured in samples collected at the Cape Grim Observatory (Smithton, Tasmania, Australia) since 1978 [*Trudinger et al.*, 2016; *Montzka et al.*, 2015], and based on the expected relationship between the Southern Hemisphere and Northern Hemisphere mixing ratios the Cape Grim time series were adjusted by 6 months to represent stratospheric entry values (Figure 8). In Figure 9a the mean ages calculated from aircraft measurements of SF_6, C_3F_8, and HFC-227ea are shown relative to normalized measurements of CFC-11 based on flights from Kiruna, Sweden, in January–March of 2010 [*Laube et al.*, 2013]. CFC-11 mixing ratios were normalized by the global average surface mixing ratios at the time of the flights and were used as an indicator of polar vortex air. Most of the aircraft measurements were taken in the 17–20 km altitude range, both inside and outside the polar vortex, and the low CFC-11 values indicate where the flights sampled vortex air. It is clearly apparent from these measurement-based mean ages that at values of normalized CFC-11 less than roughly 0.5, which is an indicator of polar vortex air at the flight altitudes, both the SF_6 and HFC-227ea mean ages are similar and significantly older than the C_3F_8-based mean ages. The differences between SF_6 mean ages and the mean ages based on the other tracers are quantified in Figure 9b. Included in Figure 9b are the differences between SF_6 and CO_2 mean ages as a function of normalized CFC-11 from the 5 March 2000 balloon flight. The differences between SF_6 mean ages and the very long lived tracers CO_2 and C_3F_8 increase as CFC-11 decreases and are in good agreement at all CFC-11 values. This indicates that CO_2 and C_3F_8 are both suitable to infer mean ages, although there are far fewer measurements of C_3F_8 to assess how well mean ages derived from the two species agree throughout the stratosphere. In contrast, the near zero differences between the SF_6 and HFC-227ea mean ages at all CFC-11 values suggest these species underwent relatively similar amounts of loss. Based on the similar amount of loss we expect these species to hav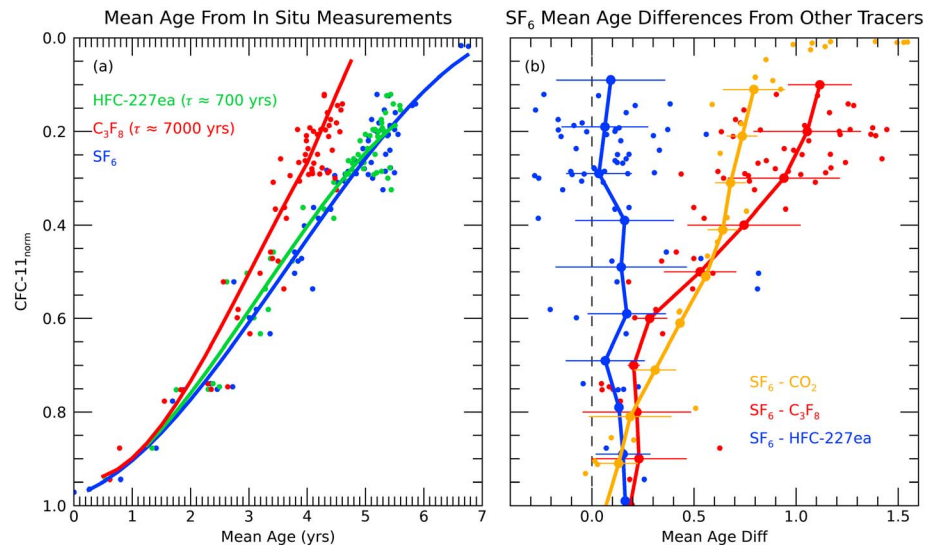e similar atmospheric lifetimes. The estimated lifetime of HFC-227ea is 670–780 years [*SPARC*, 2013], which is in good agreement with the lower end of our SF_6 lifetime estimate.

Based on these findings, we also reassess the recent estimate of the stratospheric lifetime for HFC-227ea of 370 years (range: 330 to 490 years) estimated in *Laube et al.* [2010]. This estimate was based on an earlier tropospheric trend derived from firn air, which was extrapolated forward in time. The firn air estimates of HFC-227ea were biased high by 2–20% relative to the Cape Grim values shown in Figure 8. In addition this estimate was based on a correlation with SF_6 with mixing ratios of the latter assumed to have experienced

Figure 8. Time series of the estimated global average surface mixing ratios of C_3F_8 (red) and HFC-227ea (green) based on measurements from the Cape Grim Observatory (Tasmania, Australia).

Figure 9. (a) Mean ages calculated from SF_6, C_3F_8, and HFC-227ea in situ measurements from high northern latitude aircraft flights in January–March 2010. The mean ages are plotted as a function of CFC-11 normalized to the tropical average mixing ratio at the surface at the time of the measurements. (b) Differences between mean age calculated from SF_6 and that calculated from C_3F_8, HFC-227ea, and CO_2 as a function of normalized CFC-11. The C_3F_8 and HFC-227ea mean age differences are from the aircraft data shown in Figure 9a, while the CO_2 mean age differences are from the 5 March 2000 balloon flight shown in Figure 2. The error bars are the standard deviations of the mean age differences within each CFC-11 bin.

no loss. The evidence presented in this work demonstrates that this is not the case. When using updated Cape Grim-based tropospheric trends, which are in good agreement with NOAA observations of the two gases at the same location, the stratospheric lifetimes of SF_6 and HFC-227ea are indistinguishable within uncertainties. This highlights the importance of high-precision long-term tropospheric records for stratospheric trace gas measurements, which is even more crucial when these are to be used to calculate mean ages of air.

4. Conclusions and Summary

In this paper we have derived a revised atmospheric lifetime of SF_6 of 850 years with a possible range of 580–1400 years based on in situ measurements in the stratospheric polar vortex. This is much less than the current widely used estimate of 3200 years but still within the possible range of 580 to 10,000 years reported in *Ravishankara et al.* [1993]. It is most likely that the SF_6 lifetime is in the lower end of our range, roughly 600–800 years, based on three main lines of supporting evidence. First, air that experienced SF_6 loss but that did not descend into the stratospheric polar vortex is not included in our estimate, and any additional SF_6 loss would necessarily lower our lifetime estimate. Second, the good agreement between SF_6- and HFC-227ea-based mean ages at all locations, including in the polar vortex, suggests that these two trace gases have similar fractional loss and thus similar lifetimes. The lifetime of HFC-227ea is estimated to be 670–780 years [*SPARC*, 2013], which agrees well with the lower range of calculated SF_6 lifetimes. Third, previous studies have suggested electron attachment in the mesosphere as an important loss process of SF_6 and already estimated that including this loss in models resulted in SF_6 lifetimes of 580–800 years [*Ravishankara et al.*, 1993; *Morris et al.*, 1995; *Reddmann et al.*, 2001; *Totterdill et al.*, 2015]. Our comparison with WACCM output that only includes SF_6 loss due to photolysis shows that this cannot be the dominant loss process, thus supporting the important role of electron attachment in SF_6 destruction.

The reduction of the best estimate of the SF_6 lifetime from 3200 to 850 years will have an impact on our understanding of the role of this molecule in the climate system, although the impact depends on the time horizon considered. The current value of the global warming potential (GWP) of SF_6 for a 100 year time horizon is ~23,500 [*Myhre et al.*, 2013], which is the highest value of any known trace gas. With the lifetime reduction deduced here, the SF_6 GWP for a 100 year time horizon reduces by ~4%, and for a 1000 year

time horizon by ~32%. Thus, the change in climate impact of a reduced SF_6 lifetime is small for time periods up to several hundred years, but significant over time periods that are between the new and old lifetimes.

The detection of such large SF_6 loss in the polar vortex as shown here also implies that mixing of mesospheric air into the stratosphere affects the use of SF_6 as an indicator of the mean age of stratospheric air. Based on the fact that the mass of the northern polar vortex is approximately one tenth the mass of the entire Northern Hemisphere (NH) stratosphere, if upon breakdown the polar vortex were evenly mixed with the rest of the NH stratosphere the mean ages calculated from SF_6 would be biased old by ~0.75 years above 30 km altitude and ~0.1 year at 20 km. Since the polar vortex is not evenly mixed with the rest of the stratosphere upon breakdown, the observed SF_6 mean age bias is typically less than 0.25 years in the tropics and midlatitudes [e.g., *Andrews et al.*, 2001; *Engel et al.*, 2002, 2009; *Ray et al.*, 2014]. Higher mean age biases, of 1 year or more as in this study, have been observed in high latitudes either in the polar vortex or in vortex remnants [e.g., *Strunk et al.*, 2000; *Moore et al.*, 2003; *Engel et al.*, 2006].

Finally, it is important to note that the calculation of the global atmospheric lifetime of a trace gas based on a single balloon profile is rather remarkable and shows the high leverage of well-timed and well-placed in situ measurements of key trace gases. The stratospheric polar vortices are regions of concentrated, isolated, and horizontally well mixed descent of 2 to 4 times the entire mass of the mesosphere twice each year. Polar vortex measurements have typically focused on the important aspect of ozone depletion, but this study points out that vortex measurements of certain trace gases can also be useful for understanding large-scale transport and photochemistry of the entire mesosphere and stratosphere. A measurement program such as described in *Moore et al.* [2014] would result in regular sampling in this region and allow further analysis of the type shown here.

References

Andrews, A., et al. (2001), Mean ages of stratospheric air derived from in situ observations of CO_2, CH_4 and N_2O, *J. Geophys. Res.*, *106*, 32,295–32,314, doi:10.1029/2001JD000465.

Carpenter, L. J., S. Reimann, J. B. Burkholder, C. Clerbaux, B. D. Hall, R. Hossaini, J. C. Laube, and S. A. Yvon-Lewis (2014), Ozone-depleting substances (ODSs) and other gases of interest to the Montreal Protocol, Chapter 1 in Scientific Assessment of Ozone Depletion: 2014, *Global Ozone Research and Monitoring Project – Rep. No. 55*, World Meteorol. Org., Geneva, Switzerland.

Cooperative Global Atmospheric Data Integration Project (2013), Multi-laboratory compilation of synchronized and gap-filled atmospheric carbon dioxide records for the period 1979–2012 (obspack_co2_1_GLOBALVIEW-CO2_2013_v1.0.4_2013-12-23), Compiled by NOAA Global Monitoring Division: Boulder, Colo., Data product accessed at doi:10.3334/OBSPACK/1002. [Updated annually.]

Daube, B. C., K. A. Boering, A. E. Andrews, and S. C. Wofsy (2002), A high-precision fast-response airborne CO_2 analyzer for in situ sampling from the surface to the middle stratosphere, *J. Atmos. Oceanic Technol.*, *19*, 1532–1543.

Dlugokencky, E. J., B. D. Hall, M. J. Crotwell, S. A. Montzka, G. Dutton, J. Mühle, and J. W. Elkins (2016), 1. Long-lived greenhouse gases, in "State of the Climate in 2015", (edited by D. S. Arndt, J. Blunden, and K. W. Willett), *Bull. Am. Meteorol. Soc.*, *97*(8), S44–S46, doi:10.1175/2016BAMSStateoftheClimate.1.

Dunkerton, T. J., C.-P. Hsu, and M. E. McIntyre (1981), Some Eulerian and Lagrangian diagnostics for a model warming, *J. Atmos. Sci.*, *38*, 819–843.

Engel, A., M. Strunk, M. Muller, H. P. Haase, C. Poss, I. Levin, and U. Schmidt (2002), Temporal development of total chlorine in the high-latitude stratosphere based on reference distributions of mean age derived from CO_2 and SF_6, *J. Geophys. Res.*, *107*(D12), 4136, doi:10.1029/2001JD000584.

Engel, A., et al. (2006), Observation of mesospheric air inside the Arctic stratospheric polar vortex in early 2003, *Atmos. Chem. Phys.*, *6*, 267–282, doi:10.5194/acp-6-267-2006.

Engel, A., et al. (2009), Age of stratospheric air unchanged within uncertainties over the past 30 years, *Nat. Geosci.*, *2*, 28–31, doi:10.1038/ngeo388.

Eyring, V., et al. (2013), *Overview of IGAC/SPARC Chemistry-Climate Model Initiative (CCMI) Community Simulations in Support of Upcoming Ozone and Climate Assessments*, vol. 40, pp. 48–66, SPARC newsletter, Zurich, Switzerland.

Fisher, M., A. O'Neill, and R. Sutton (1993), Rapid descent of mesospheric air into the stratospheric polar vortex, *Geophys. Res. Lett.*, *20*, 1267–1270, doi:10.1029/93GL01104.

Gao, R. S., et al. (2002), Role of NO_y as a diagnostic of small-scale mixing in a denitrified polar vortex, *J. Geophys. Res.*, *107*(D24), 4794, doi:10.1029/2002JD002332.

Garcia, R. R., A. K. Smith, D. E. Kinnison, Á. de la Cámara, and D. Murphy (2017), Modification of the gravity wave parameterization in the Whole Atmosphere Community Climate Model: Motivation and results, *J. Atmos. Sci.*, doi:10.1175/JAS-D-0104.1.

Haenel, F. J., et al. (2015), Reassessment of MIPAS age of air trends and variability, *Atmos. Chem. Phys.*, *15*, 13,161–13,176, doi:10.5194/acpd-15-14685-2015.

Hall, B. D., S. A. Montzka, G. Dutton, and J. W. Elkins (2016), 2. Ozone-depleting gases, in State of the Climate in 2015, *Bull. Am. Meteorol. Soc.*, *97*(8), S47–S48, doi:10.1175/2016BAMSStateoftheClimate.1.

Hall, T. M., and R. A. Plumb (1994), Age as a diagnostic of stratospheric transport, *J. Geophys. Res.*, *99*, 1059–1070, doi:10.1029/93JD03192.

Harries, J. E., S. Ruth, and J. M. Russell III (1996), On the distribution of mesospheric molecular hydrogen inferred from HALOE measurements of H_2O and CH_4, *Geophys. Res. Lett.*, *23*, 297–300, doi:10.1029/95GL03197.

Harvey, V. L., R. B. Pierce, and M. H. Hitchman (2002), A climatology of stratospheric polar vortices and anticyclones, *J. Geophys. Res.*, *107*(D20), 4442, doi:10.1029/2001JD001471.

Haynes, P., and E. Shuckburgh (2000), Effective diffusivity as a diagnostic of atmospheric transport: 1. Stratosphere, *J. Geophys. Res.*, *105*, 22,777–22,794, doi:10.1029/2000JD900093.

Hodnebrog, O., M. Etminan, J. S. Fuglestvedt, G. Marston, G. Myhre, C. J. Nielsen, K. P. Shine, and T. J. Wallington (2013), Global warming potentials and radiative efficiencies of halocarbons and related compounds: A comprehensive review, *Rev. Geophys.*, *51*, 300–378, doi:10.1002/rog.20013.

Hurrell, J. W., et al. (2013), The Community Earth System Model: A framework for collaborative research, *Bull. Am. Meteorol. Soc.*, *94*, 1339–1360, doi:10.1175/BAMS-D-12-00121.1.

Kida, H. (1983), General circulation of air parcels and transport characteristics derived from a hemispheric GCM part 2. Very long-term motions of air parcels in the troposphere and stratosphere, *J. Meteorol. Soc. Jpn.*, *61*, 510–522.

Kovács, T., et al. (2017), Determination of the atmospheric lifetime and global warming potential of sulfur hexafluoride using a three-dimensional model, *Atmos. Chem. Phys.*, *17*(2), 883–898, doi:10.5194/acp-17-883-2017.

Laube, J. C., et al. (2010), Accelerating growth of HFC-227ea (1,1,1,2,3,3,3-heptafluoropropane) in the atmosphere, *Atmos. Chem. Phys.*, *10*, 5903–5910.

Laube, J. C., A. Keil, H. Bönisch, A. Engel, T. Röckmann, C. M. Volk, and W. T. Sturges (2013), Observation-based assessment of stratospheric fractional release, lifetimes, and ozone depletion potentials of ten important source gases, *Atmos. Chem. Phys.*, *13*, 2779–2791.

Lean, J., G. Rottman, J. Harder, and G. Kopp (2005), SORCE contributions to new understanding of global change and solar variability, *Sol. Phys.*, *230*, 27–53, doi:10.1007/s11207-005-1527-2.

Manney, G. L., and Z. D. Lawrence (2016), The major stratospheric final warming in 2016: Dispersal of vortex air and termination of Arctic chemical ozone loss, *Atmos. Chem. Phys.*, *16*, doi:10.5194/acp-16-15371-2016.

Manney, G. L., and J. L. Sabutis (2000), Development of the polar vortex in the 1999–2000 Arctic winter stratosphere, *Geophys. Res. Lett.*, *27*, 2589–2592.

Marsh, D. R. M. J., D. E. Mills, J. F. Kinnison, N. C. Lamarque, and L. M. Polvani (2013), Climate change from 1850 to 2005 simulated in CESM1 (WACCM), *J. Clim.*, *26*, 7372–7391, doi:10.1175/JCLI-D-12-00558.1.

Minschwaner, K., et al. (2010), The photochemistry of carbon monoxide in the stratosphere and mesosphere evaluated from observations by the Microwave Limb Sounder on the Aura satellite, *J. Geophys. Res.*, *115*, D13303, doi:10.1029/2009JD012654.

Montzka, S. A., M. McFarland, S. O. Andersen, B. R. Miller, D. W. Fahey, B. D. Hall, L. Hu, C. Siso, and J. W. Elkins (2015), Recent trends in global emissions of hydrochlorofluorocarbons and hydrofluorocarbons: Reflecting on the 2007 adjustments to the Montreal Protocol, *J. Phys. Chem. A*, *119*, doi:10.1021/jp5097376.

Moore, F. L., et al. (2003), Balloonborne in situ gas chromatograph for measurements in the troposphere and stratosphere, *J. Geophys. Res.*, *108*(D5), 8330, doi:10.1029/2001JD000891.

Moore, F. L., E. A. Ray, K. H. Rosenlof, J. W. Elkins, P. Tans, A. Karion, and C. Sweeney (2014), A cost effective trace gas measurement program for long term monitoring of the stratospheric circulation, *Bull. Am. Meteorol. Soc.*, doi:10.1175/BAMS-D-12-00153.1.

Morris, R. A., T. M. Miller, A. A. Viggiano, J. F. Paulson, S. Solomon, and G. Reid (1995), Effects of electron and ion reactions on atmospheric lifetimes of fully fluorinated compounds, *J. Geophys. Res.*, *100*, 1287–1294, doi:10.1029/94JD02399.

Myhre, G., et al. (2013), Anthropogenic and natural radiative forcing supplementary material, in *Climate Change 2013: The Physical Science Basis. Contribution of Working Group I to the Fifth Assessment Report of the Intergovernmental Panel on Climate Change*, edited by T. F. Stocker et al., Cambridge Univ. Press, Cambridge, U. K., and New York.

Plumb, R. A., W. Heres, J. L. Neu, N. M. Mahowald, J. del Corral, G. C. Toon, E. Ray, F. Moore, and A. E. Andrews (2003), Global tracer modeling during SOLVE: High latitude descent and mixing, *J. Geophys. Res.*, *108*(D5), 8309, doi:10.1002/2001JD001023.

Pradayrol, C., A. M. Casanovas, I. Deharo, J. P. Guelfucci, and J. Casanovas (1996), Absorption coefficients of SF_6, SF_4, SOF_2, and SO_2F_2 in the vacuum ultraviolet, *J. Phys. III France*, *6*, 603–612, doi:10.1051/jp3:1996143.

Ravishankara, A. R., S. Solomon, A. A. Turnipseed, and R. F. Warren (1993), Atmospheric lifetimes of long-lived halogenated species, *Science*, *259*, 194–199, doi:10.1126/science.259.5092.194.

Ray, E. A., F. L. Moore, J. W. Elkins, D. F. Hurst, P. A. Romashkin, G. S. Dutton, and D. W. Fahey (2002), Descent and mixing in the 1999-2000 northern polar vortex inferred from in situ tracer measurements, *J. Geophys. Res.*, *107*(D20), 8285, doi:10.1002/2001JD000961.

Ray, E. A., et al. (2014), Improving stratospheric transport trend analysis based on SF_6 and CO_2 measurements, *J. Geophys. Res. Atmos.*, *119*, 14,110–14,128, doi:10.1002/2014JD021802.

Reddmann, T., R. Ruhnke, and W. Kouker (2001), Three-dimensional model simulations of SF_6 with mesospheric chemistry, *J. Geophys. Res.*, *106*, 14,525–14,537, doi:10.1029/2000JD900700.

Rienecker, M. M., et al. (2011), MERRA: NASA's Modern-Era Retrospective Analysis for Research and Applications, *J. Clim.*, *24*, 3624–3648, doi:10.1175/JCLI-D-11-00015.1.

Schmidt, U., and A. Khedim (1991), In situ measurements of carbon dioxide in the winter arctic vortex and at midlatitudes: An indicator of the 'age' of stratospheric air, *Geophys. Res. Lett.*, *18*, 763–766, doi:10.1029/91GL00022.

Solomon, S., D. Kinnison, J. Bandoro, and R. Garcia (2015), Simulation of polar ozone depletion: An update, *J. Geophys. Res. Atmos.*, *120*, 7958–7974, doi:10.1002/2015JD023365.

Stratospheric Processes and their Role in Climate (SPARC) (2013), SPARC Report on the lifetimes of stratospheric ozone-depleting substances, their replacements, and related species, edited by M. K. W. Ko, P. A. Newman, S. Reimann, S. E. Strahan, *SPARC Rep. 6, WCRP–15/2013*. [Available at www.sparc-climate.org/publications/sparc-reports/.]

Strunk, M., A. Engel, U. Schmidt, C. M. Volk, T. Wetter, I. Levin, and H. Glatzer-Mattheier (2000), CO_2 and SF_6 as stratospheric age tracers: Consistency and the effect of mesospheric SF_6-loss, *Geophys. Res. Lett.*, *27*, 341–344, doi:10.1029/1999GL011044.

Totterdill, A., T. Kovács, J. C. Gómez Martín, W. Feng, and J. M. C. Plane (2015), Mesospheric removal of very long-lived greenhouse gases SF_6 and CFC-115 by metal reactions, Lyman-α photolysis, and electron attachment, *J. Phys. Chem.*, *119*, 2016–2025, doi:10.1021/jp5123344.

Trudinger, C. M., et al. (2016), Atmospheric abundance and global emissions of perfluorocarbons CF_4, C_2F_6 and C_3F_8 since 1800 inferred from ice core, firn, air archive and in situ measurements, *Atmos. Chem. Phys.*, *16*, doi:10.5194/acp-16-11733-2016.

Volk, C. M., J. W. Elkins, D. W. Fahey, G. S. Dutton, J. M. Gilligan, M. Loewenstein, J. R. Podolske, K. R. Chan, and M. R. Gunson (1997), Evaluation of source gas lifetimes from stratospheric observations, *J. Geophys. Res.*, *102*, 24,543–24,564, doi:10.1029/97JD02215.

Von Hobe, M., et al. (2013), Reconciliation of essential process parameters for an enhanced predictability of Arctic stratospheric ozone loss and its climate interactions (RECONCILE): Activities and results, *Atmos. Chem. Phys.*, *13*, 9233–9268, doi:10.5194/acp-13-9233-2103.

Waugh, D. W. and T. M. Hall (2002), Age of stratospheric air: Theory, observations and models, *Rev. Geophys.*, *40*(4), 1010, doi:10.1029/2000RG000101.